NIH Public Access
Author Manuscript
Biochemistry. Author manuscript; available in PMC 2014 January 08.

Published in final edited form as:
Biochemistry. 2013 January 8; 52(1): 84–97. doi:10.1021/bi300886q.

The Effects of Select Histidine to Cysteine Mutations on Transcriptional Regulation by *E. coli* RcnR‡

Khadine A. Higgins[†,#], **Heidi Q. Hu**[‡], **Peter T. Chivers**[^], and **Michael J. Maroney**[†,‡,*]

[†]Department of Chemistry, University of Massachusetts, Amherst, Massachusetts 01003

[‡]Program in Molecular and Cellular Biology, University of Massachusetts, Amherst, Massachusetts 01003

Department of Biochemistry and Molecular Biophysics, Washington University School of Medicine, St. Louis, Missouri 63110

Abstract

The RcnR metalloregulator represses the transcription of the Co(II) and Ni(II) exporter, RcnAB. Previous studies have shown that Co(II) and Ni(II) bind to RcnR in six-coordinate sites, resulting in de-repression. Here, the roles of His60, His64, and His67 in specific metal recognition are examined. His60 and His64 correspond to ligands that are important for Cu(I) binding in the homologous Cu(I)-responsive metalloregulator, CsoR. These residues are known to be functionally important in RcnR transcriptional regulation. XAS was used to examine the structure of bound cognate and non-cognate metal ions, and *lacZ* reporter assays were used to assess the transcription of *rcnA* in response to metal binding in the three His → Cys mutations, H60C, H64C and H67C. These studies confirm that both Ni(II) and Co(II) use His64 as a ligand. H64C-RcnR is also the only known mutation that retains a Co(II) response while eliminating the response to Ni(II) binding. XAS data indicate that His60 and His67 are potential Co(II) ligands. The effects of the mutations of His60, His64, and His67 residues on the structures of the non-cognate metal ions (Zn(II) and Cu(I)) reveals that these residues have distinctive roles in binding non-cognate metals. None of the His → Cys mutants in RcnR confer any response to Cu(I) binding, including H64C-RcnR, where the ligands involved in Cu(I) binding in CsoR are present. These data indicate that while the secondary, tertiary and quaternary structures of CsoR and RcnR are quite similar, small changes in primary sequence reveal that the specific mechanisms involved in metal recognition are quite different.

Transition metal ions are essential cofactors for many enzymes and proteins that carry out a variety of processes (1). Excessively high concentrations of these metal ions can have severe

‡This work was supported by NIH grant R01-GM069696 to MJM and NSF MCB0520877 to PTC. XAS data collection at the National Synchrotron Light Source at Brookhaven National Laboratory was supported by the U.S. Department of Energy, Division of Materials Sciences and Division of Chemical Sciences. Beam line X3B at NSLS is supported by the NIH. This publication was made possible by the Center for Synchrotron Biosciences grant, P30-EB-009998, from the National Institute of Biomedical Imaging and Bioengineering (NIBIB). Portions of this research were carried out at the Stanford Synchrotron Radiation Light source, a national user facility operated by Stanford University on behalf of the U.S. Department of Energy, Office of Basic Energy Sciences. The SSRL Structural Molecular Biology Program is supported by the Department of Energy, Office of Biological and Environmental Research, and by the National Institutes of Health, National Center for Research Resources, Biomedical Technology Program.

[*]413-545-6876, mmaroney@chemistry.umass.edu.
[#]Current Address: Department of Chemistry, Indiana University, Bloomington, IN 47405
[^]Current Address: Department of Chemistry and Biochemistry, Oberlin College, Oberlin, OH 44074

Supporting Information
Table of mutagenic primers used for the H60C, H64C and H67C mutants. EPR spectra of Cu(I) H60C-, H64C-, H67C-RcnR and Cu(II)-EDTA. *lacZ* reporter assay of H64C-RcnR. Tables with additional XAS fits for wild-type and mutant RcnR proteins. This material is available free of charge via the Internet at http://pubs.acs.org.

NIH-PA Author Manuscript
NIH-PA Author Manuscript
NIH-PA Author Manuscript

NIH-PA Author Manuscript

NIH-PA Author Manuscript

NIH-PA Author Manuscript

effects on cellular metabolism (2). For this reason, the levels of metal ions in cells need to be tightly regulated. Cellular trafficking systems for transition metals are equipped with importers, exporters, chaperones and accessory proteins involved in metallocenter assembly, and transcriptional regulators that respond to specific transition metals. It is essential for trafficking systems to be selective for their cognate metals in order to generate a metal-specific biological response.

The nickel trafficking pathway in *E. coli* supplies nickel for hydrogenase active site assembly (3, 4), and consists of the importer NikABCDE (5, 6), a nickel metallochaperone (HypA) (7, 8) and other proteins that bind nickel and are involved in hydrogenase active site assembly (*e.g.*, HypB and SlyD) (7, 9, 10), and an exporter RcnAB (11–13). Two transcriptional regulators, NikR (14, 15) (for NikABCDE) and RcnR (16) (for RcnAB) work together to regulate the expression of the importer and the exporter and to maintain nickel homeostasis (16). Genetic data obtained by Iwig *et al.* (16) indicate that RcnA is important for H_2ase3 activity by modulating NikR. RcnR and CsoR, a copper-responsive transcriptional regulator that represses *cso* that encodes a P-type ATPase for efflux of copper and a gene of unknown function, constitute a new structural class of transcriptional regulators characterized by an all α-helical structure in a four-helix bundle (17, 18). *E. coli* RcnR is a 40 kDa tetrameric nickel- and cobalt-responsive transcriptional repressor (16). The apo-protein recognizes a TACT-G_6-N-AGTA DNA motif, of which there are two located in the *rcnA-rcnR* intergenic region (19). Apo-RcnR binds to DNA repressing the transcription of *rcnAB*, the genes encoding nickel and cobalt efflux proteins, RcnAB (11). RcnR also interacts with flanking DNA regions of ~50 base pairs, leading to DNA wrapping (19). DNA binding is disfavored by the binding of one equivalent of Ni(II) or Co(II) to RcnR, four per tetramer (16, 20), allowing for the transcription of the RcnAB exporter under conditions of excess metal. In addition to controlling the transcription of *rcnAB*, RcnR also controls the transcription of its own gene (20), as does CsoR (17).

The structurally related copper-responsive metalloregulator, CsoR, has been crystallographically characterized as an apo-protein from *T. thermophilus* (21) and *S. lividans* (22) as well as a Cu(I) complex using protein from *M. tuberculosis* (17). These structures show that the protein adopts an all α-helical dimer of dimers architecture. In the complex, Cu(I) is coordinated by two cysteine residues, Cys36 from one subunit and Cys65 from another subunit as well as histidine residue, His61, from the same subunit as Cys65 (17). Binding of Cu(I) to CsoR negatively regulates the interaction between CsoR and the operator-promoter region of the *cso* operon (17), presumably by disfavoring the DNA binding conformation. However, in the absence of a structure of the DNA complex, the details of how this occurs are unknown. Recently a new member of the CsoR/RcnR family of protein was discovered in *Synechocystis* PCC 6803, InrS (23). InrS is a Ni(II)-responsive transcriptional regulator that represses the transcription of *nrsD,* which encodes a Ni(II) efflux protein (23). InrS binds Co(II), Ni(II) and Cu(I) and contains the Cu(I) binding ligands found in CsoR (Figure 1). However, InrS is responsive to binding Ni(II), and not responsive to Cu(I) binding. UV-vis data determined that the metal site structures of InrS are more similar to CsoR than RcnR (23–26); the nickel site is four-coordinate with planar geometry (23).

There is no crystal structure of RcnR, but data regarding the metal site structures obtained from XAS studies have established that the details of the metal binding are distinct from CsoR (24, 25). RcnR forms six-coordinate $M(N/O)_5S$ complexes with its cognate metal ions (Ni(II) and Co(II)), employing the single Cys that is conserved in the RcnR family of proteins (Cys35, homologous with Cys36 in CsoR) to bind both cognate metals (24). Non-cognate metal ions (*e.g.,* Cu(I) and Zn(II)) are bound to RcnR by three protein ligands with an $(N/O)_2S$ donor atom set, and may also incorporate an anion from the buffer (25). One of

NIH-PA Author Manuscript

NIH-PA Author Manuscript

NIH-PA Author Manuscript

the ligands missing from the non-cognate sites is the N-terminal amine, which is bound to both cognate metals, and the side chain of His3, which is a ligand only for Co(II) (25). The Co(II) and Ni(II) sites are therefore distinguished by their histidine coordination, as well as by the M-S bond distance (2.31 Å for Co(II) vs. 2.62 Å for Ni(II)) (24, 25). *E. coli* RcnR possesses five histidine residues: His3, His33, His60, His64 and His67 (Figure 1). All five histidine residues were mutated by Iwig *et al.* (24), who showed using a *lacZ* reporter assay that the three conserved residues in RcnR, His3, His60 and His64, are required for full sensitivity to Co(II) binding, while only His3 and His64 were required for full sensitivity to Ni(II) binding. The mutations of the non-conserved His33 and His67 had no significant effect on either the Co(II) or Ni(II) transcriptional response in cells (24). However, these functional studies do not distinguish whether these His residues directly coordinate cognate or non-cognate metals or which His residues might bind only to certain metals as all of these mutations involved sidechains that are not expected to coordinate metals (Ala, Leu, Asn, or Arg) (24). To gain improved insight into Ni(II), Co(II) and non-cognate metal binding, His → Cys mutations were made with the expectation that the additional S-donor ligand would be apparent in the EXAFS spectrum if the substituted His residue is indeed a ligand. Additionally, CsoR possesses one His and two Cys ligands that are used to coordinate Cu(I), so it is possible that a change in metal recognition might be promulgated by creating the Cu(I) ligand set of CsoR in RcnR (the H64C mutant). The metal site structures for Co(II), Ni(II), Cu(I) and Zn(II) complexes of the mutant proteins were then characterized using XAS, and the response of the mutant proteins to various metal ions was determined by using *lacZ* reporter assays. These studies provide additional insight into the role of His ligation in cognate and non-cognate metal complexes, although surprisingly the mutant proteins failed to produce a Cu(I) sensor or even CsoR-like Cu(I) coordination, indicating that there is more complexity to metal responsiveness besides the coordination number, ligands employed, and their position in the protein amino acid sequence even in this simple helical bundle structural scaffold.

Experimental Procedures

RcnR Mutagenesis

Point mutations of the His60, His64 or His67 to Cys were made in the wild-type RcnR plasmid (24) using QuikChange™ Site Directed Mutagenesis Kit (Stratagene). Primers used in the PCR reactions are shown in the Supporting Information, Table S1. The PCR product was transformed into NovaBlue (Novagen) competent cells. The cells were then grown on LB/agar plates overnight, a single colony was selected and grown overnight in a 5 mL culture (LB amp media). The DNA was isolated using the Qiagen® miniprep kit and sequenced at GENEWIZ Inc. (South Plainfield, NJ) to confirm that the correct mutation was present.

RcnR Overexpression and Purification

Single colonies of *E. coli* DL41 (DE3) pLysS cells containing the plasmid encoding H60C-, H64C- and H67C-RcnR mutant proteins were grown in 150 mL Luria-Bertani broth (LB) cultures, supplemented with 30 μg/mL cam and 100 μg/mL amp overnight at 37 °C with shaking. An aliquot (20 mL) of the overnight culture was added to 2 L of fresh LB with cam and amp. The cultures were grown to an OD_{600} of ~0.8 and then induced by addition of IPTG to a final concentration of 0.8 mM. The cells were harvested after 3 hours by centrifugation (~8000 g for 20 minutes), resuspended in residual media, and frozen at −80 °C. The cells were lysed upon thawing in a water bath at 37 °C and treated with 10 μL of a DNAse I solution (10 mg/ml DNAse I, 40% glycerol), 1.5 mM (final concentration) of PMSF (MP Biomedicals) and 5 mM (final concentration) TCEP (Thermo Scientific). The mixture was then incubated at 37 °C for half an hour.

NIH-PA Author Manuscript

NIH-PA Author Manuscript

NIH-PA Author Manuscript

All chromatographic purifications employed an AKTA-FPLC system (Amersham Biosciences) and were carried out at room temperature. The lysed cells were centrifuged (~6000 g for 30 minutes) and the lysate applied to a SP sepharose column (18 mL) equilibrated with 20 mM Hepes (pH 7.0), 1 mM TCEP, 5 mM EDTA, 10% glycerol, 50 mM NaCl (buffer A). The column was washed with 50 mL of buffer A followed by a linear gradient from 0–100% of buffer B (20 mM Hepes (pH 7.0), 1 mM TCEP, 5 mM EDTA, 10% glycerol, 1 M NaCl), total volume 117 mL at a flow rate of 2 mL/minute while collecting 5 mL fractions. A sodium dodecyl sulfate polyacrylamide electrophoresis (SDS-PAGE) gel was run to determine the fractions containing RcnR; RcnR eluted between ~35–55% buffer B. These fractions were combined, concentrated to 4 mL and loaded on a HiLoad 16/60 Superdex 200 (GE Life Sciences) column equilibrated with buffer C (20 mM Hepes (pH 7.0), 1 mM TCEP, 5 mM EDTA, 10% glycerol, 300 mM NaCl). One column volume (120 mL) of buffer C was run over the column at a flow rate of 0.7 mL/min, fractions were collected based on absorbance at 280 nm. Protein fractions with an absorbance > 10 mAU were collected in 2 mL fractions. Following this column, a SDS-PAGE gel was run to determine the fractions that contained RcnR; RcnR eluted as a single peak at a volume consistent with that of a tetramer. These RcnR fractions were concentrated and buffer exchanged into buffer A. A MonoS 5/50 GL column (GE Life Sciences) was equilibrated with buffer A before loading 20 mL of the protein in buffer A. The column was washed with 20 mL of buffer A, followed by a linear gradient of 0–100% buffer B over 40 mL at a flow rate of 1.5 mL/minute while collecting 2 mL fractions. The purity of the fractions was checked using SDS-PAGE gel; RcnR eluted as a single peak at ~15–30% buffer B. Pure fractions of RcnR were pooled together and stored at 4 °C. Molecular weights of the expressed proteins were determined by electrospray ionization mass spectrometry (ESI-MS) using a Bruker Esquire instrument equipped with an HP-HPLC (Agilent) for the removal of salt present in the protein solutions. The molecular weight of expressed proteins was determined by ESI-MS and confirm the presence of the His → Cys mutation in each case (calculated mass for each is 9969 Da; the mass obtained from mass spectrometry was: 9967 Da for H60C-RcnR, 9967 Da for H64C-RcnR and 9970 Da for H67C-RcnR). The molecular weights obtained are also consistent with the loss of the N-terminal methionine residue, as seen for the wild-type protein and all the previously characterized mutations (24, 25).

Metal Complexes of RcnR Proteins

The proteins were concentrated to ~150 μM and desalted twice using a buffer containing 20 mM Hepes (pH 7.0), 10% glycerol and 300 mM NaBr, NaCl or NaOAc salts (buffer M) using Zebra spin desalting columns, 7K MWCO, 10 mL (Pierce) to remove EDTA and TCEP. In the case of the Cu(I) samples, the final buffer also contained 2 mM TCEP. Buffer containing either NaOAc or NaCl were used in some cases to confirm the binding of exogenous buffer ligands. The protein concentrations were determined by using the experimentally determined extinction coefficient of $\varepsilon_{276} = 2530\ M^{-1}\ cm^{-1}$ from protein denatured with 8 M guanidine hydrochloride (24). Two to three equivalents of aqueous 10 mM stock solutions of $CoCl_2{\bullet}6H_2O$, $NiCl_2{\bullet}6H_2O$, $Zn(CH_3COO)_2{\bullet}2H_2O$, $Cu(CH_3COO)_2{\bullet}H_2O$ (Fisher Scientific) or $[(CH_3CN)_4Cu]PF_6$ (Aldrich) salts were then added to the RcnR solutions to prepare the respective complexes. These samples were allowed to equilibrate overnight before incubation with Chelex™ beads for ~30 minutes to remove any nonspecifically bound metal ions.

Cu(I)-RcnR was prepared under anaerobic conditions. Air was removed from the protein solution on a Schlenk line by alternating between argon and vacuum five times. The protein was then placed into a Coy (Coy Laboratory Products Inc., Grass Lakes, MI) anaerobic chamber (90% N_2 and 10% H_2) and incubated with three equivalents of a 10 mM

NIH-PA Author Manuscript

NIH-PA Author Manuscript

NIH-PA Author Manuscript

$(CH_3CN)_4CuPF_6$ solution (nitrogen saturated anaerobic solution of 10 % acetonitrile in water) overnight. Chelex™ beads were added to the solution to remove any nonspecifically bound metal ions. The oxidation state of the Cu(I) samples were verified using X-band EPR (Bruker ELEXSYS E-500 X-band spectrometer) at 77 K on the samples frozen in XAS holders and inserted into a finger dewar. The percentage of Cu(II) present in the sample was determined by comparing the second integrals of the Cu(I) protein spectra with that of a 1.03 mM Cu(II)-EDTA sample used as a standard. The Cu(I) H60C-RcnR sample in buffer M with NaBr and the Cu(I) H64C-RcnR sample in buffers with NaBr and NaCl had < 1% Cu(II) present while Cu(I) H67C-RcnR in buffer M with NaBr had ~1.6% Cu(II) present (Supporting Information, Figure S1).

Based on the previously determined protein concentrations, samples of RcnR proteins containing ~1 ppm of the respective metals were prepared for metal analysis by diluting aliquots of the metal complexes to 1 mL with deionized water. The metal content was determined using a Perkin-Elmer Optima DV4300 ICP-OES instrument. The metal:protein ratios for samples prepared in buffer M with NaBr are as follows: H60C-RcnR: Co(II), 0.84:1, Ni(II) 1.17:1, Cu(I) 1.05:1, Zn(II) 1.17:1; H64C-RcnR: Co(II) 1.26:1, Ni(II) 0.59:1, Cu(I) 1.33:1, Zn(II) 1.21:1; H67C-RcnR: Co(II) 0.935:1, Ni(II) 1.21:1, Cu(I) 1.03:1, Zn(II) 1.05:1. Complexes of H64C-RcnR in buffer M with NaCl had the following metal:protein ratios: Co(II) 0.87:1, Ni(II) 0.76:1, Cu(I) 1.29:1. A sample of Zn(II)-RcnR was made in buffer M with 300 mM NaOAc and metal:protein ration of 0.95:1. Metal complexes of H60C- and H67C-RcnR proteins in buffer M with NaOAc, had metal:protein ratios: H60C-RcnR: Ni(II) 1.10:1, Zn(II) 1.00:1; H67C: Ni(II) 1.125:1, Zn(II) 0.70:1.

β-Galactosidase Reporter Experiments

β-Galactosidase reporter experiments were conducted using two plasmids as follows:(24) The chloramphenicol-resistant P_{rcnA}-*lacZ* plasmid, pJI115,(16) was transformed into the *E. coli* strain PC888 (Δ*lacZ* Δ*rcnR*) after which ampicillin-resistant plasmids expressing the H60C, H64C, or H67C RcnR proteins were transformed into the strain. This strain background provides for low-level expression of the RcnR proteins. To assay reporter activity, the transformed cells were grown anaerobically in medium containing ampicillin and chloramphenicol with metals added at the maximal concentration for Ni(II), Co(II), Cu(II), Zn(II), or Cd(II) that resulted in < 10 % inhibition of growth (measured by final OD_{600}) – 500 μM $NiCl_2$, 150 μM $CoCl_2$, 100 μM $CuCl_2$, 300 μM $ZnCl_2$, and 50 μM $CdSO_4$ (24).

X-ray Absorption Spectroscopy (XAS)

Samples of the metallated proteins were concentrated to 1–3.2 mM (50 μL) in 20 mM Hepes (pH 7.0), 300 mM NaBr, NaCl or NaOAc with 10% glycerol using a microspin concentrator (Vivascience). The samples were syringed into polycarbonate XAS holders that were wrapped in kapton tape, and rapidly frozen in liquid nitrogen. The final concentrating and freezing of Cu(I)-RcnR was conducted under an anaerobic atmosphere in a Coy chamber.

XAS data for the RcnR protein samples were collected as previously described (28). Data was collected under dedicated ring conditions on beam line X3b at the National Synchrotron Light Source (NSLS), Brookhaven National Laboratories, with the exception of H67C-RcnR + Ni in buffer M with NaOAc, which was collected on 9-3 at Stanford Synchrotron Radiation Laboratory (SSRL). For data collection at NSLS, each sample was syringed into polycarbonate sample holders that were wrapped in kapton tape, and frozen in liquid nitrogen. The samples were loaded into an aluminum sample holder, which was cooled to ~50 K by using a He displex cryostat. Data were collected under ring conditions of 2.8 GeV and 120–300 mA using a sagittally focusing Si(111) double-crystal monochromator.

NIH-PA Author Manuscript

NIH-PA Author Manuscript

NIH-PA Author Manuscript

Harmonic rejection was accomplished with a Ni-coated focusing mirror. X-ray fluorescence was collected using a 13-element Ge detector (Canberra). Scattering was minimized by placing a Z-1 filter between the sample chamber and the detector. Additionally, for H64C-RcnR + Ni(II), H64C-RcnR + Zn(II) and H67C-RcnR + Zn(II) in buffer M containing NaCl, NaOAc and NaOAc, respectively, data were collected at NSLS using a 30-element fluorescence detector (Canberra). At SSRL, data were collected at 10 K using a liquid helium cryostat (Oxford Instruments). The ring conditions were 3 GeV and 80–100 mA. Beam line optics consisted of a Si(220) double-crystal monochromator and two rhodium coated mirrors, a flat mirror before the monochromator for harmonic rejection and vertical columnation, a second toroidal mirror after the monochromator for focusing. X-ray fluorescence was collected using a 100-element detector (Canberra). Soller slits with a Z-1 element filter were placed in between the sample chamber and the detector to minimize scattering.

XANES was collected from ± 200 eV relative to the metal edge. The X-ray energy for each metal K_α-edge was internally calibrated to the first inflection point of the corresponding metal foil: Co, 7709.5 eV; Ni, 8331.6 eV; Cu, 8980.3 eV; and Zn, 9660.7 eV. EXAFS was collected to 13.5 – 16 k above the edge energy (E_o), depending on the signal:noise at high values of k.

Data Reduction and Analysis

The XAS data reported are the average of 4–10 scans. Each XANES spectrum used in the average was analyzed for edge energy shifts that might indicate redox in the beam. None of the samples showed any significant changes. XANES and EXAFS data were analyzed using EXAFS123 (29) and SixPack (30) respectively. The SixPack fitting software builds on the ifeffit engine (31, 32). XANES analysis was carried out as described previously (28) by fitting a cubic function to the baseline in the pre-edge region of the spectra and using a 75% Gaussian and 25% Lorenzian function to fit the rise in fluorescence occurring at the edge. Transitions occurring at lower energy were fit using Gaussian functions and the areas of the Gaussians were taken to be the peak areas.

For the EXAFS analysis, each data set was background-corrected and normalized. The data were converted to k-space using the $k = [2m_e(E - E_o)/\hbar^2]^{1/2}$ relationship, where m_e is the mass of the electron, $\hbar$ is Plank's constant divided by 2π, and E_o is the threshold energy of the absorption edge. The threshold energies chosen for the metals studied were 7723 eV for Co, 8340 eV for Ni, 8990 eV for Cu and 9670 eV for Zn (28). A Fourier-transform of the data was produced using the data range $k = 2 – 12.5$ Å^{-1}, where the upper limit was determined by signal:noise. Scattering parameters for EXAFS fitting were generated using FEFF8 software package (31). The k^3-weighted data were fit in r-space. The first coordination sphere was determined by setting the number of scattering atoms in each shell to integer values and systematically varying the combination of N/O- and S-donors (Supporting Information, Tables S3 – S22).

Multiple-scattering parameters for imidazole ligands bound to various metals were generated from crystallographic coordinates using the FEFF8 software package with previously published crystal structures as input (17, 31, 33–36). The best fits resulted in four prominent multiple-scattering features and paths of similar overall lengths were combined to make four imidazole scattering paths, matching these four prominent features as outlined by Costello *et al.* (37, 38). The four combined paths were used to fit the data by setting the number of imidazole ligands per metal ion to integral values allowing r and σ^2 to vary (37, 38). This method of fitting imidazoles is an approximation; therefore, no physical label can be applied to these paths. To compare different models of the same data set, ifeffit utilizes three goodness of fit parameters: χ^2, reduced χ^2, and the R-factor. These parameters are not

NIH-PA Author Manuscript

NIH-PA Author Manuscript

NIH-PA Author Manuscript

to be confused with nomenclature where R is used for interatomic distance and χ for *k*-space EXAFS. The statistical parameter, χ^2, that is minimized in a fit, is given by equation 1, where N_{idp} is the number of independent data points, N_{ε^2} is the number of uncertainties to minimize, Re( ) denotes the real part of the EXAFS function, Im( ) is the imaginary part of the EXAFS fitting function and $\tilde{\chi}(R_i)$ is the Fourier-transformed data or model function.

$$\chi^2=\frac{N_{idp}}{N_{\varepsilon^2}}\sum_{i=1}^{N}\{[Re(\tilde{\chi}_{data}(R_i)-\tilde{\chi}_{model}(R_i))]^2+[Im(\tilde{\chi}_{data}(R_i)-\tilde{\chi}_{model}(R_i))]^2\} \quad (1)$$

Reduced $\chi^2 = \chi^2/(N_{idp} - N_{varys})$ where N_{varys} is the number of refining parameters and represents the degrees of freedom in the fit. Additionally ifeffit calculates the R-factor for each fit, which is directly proportional to χ^2 and a measure of absolute misfit between the data and theory. The R-factor is given by equation 2, and is scaled to the magnitude of the data making it proportional to χ^2.

$$R=\frac{\sum_{i=1}^{N}\{[Re(\tilde{\chi}_{data}(R_i)-\tilde{\chi}_{model}(R_i))]^2+[Im(\tilde{\chi}_{data}(R_i)-\tilde{\chi}_{model}(R_i))]\}^2}{\sum_{i=1}^{N}\{[Re(\tilde{\chi}_{data_i}(R_i))]^2+[Im(\tilde{\chi}_{data}(R_i))]^2\}} \quad (2)$$

In comparing different models, the R-factor and reduced χ^2 parameter were used to determine which model was the best fit for the data. The R-factor will always generally improve with an increasing number of adjustable parameters, while reduced χ^2 will go through a minimum and then increase, indicating that the model is over fitting the data (39).

Results

RcnR Metal Specificity in vivo

The His → Cys mutations were tested for metal responsiveness using a *lacZ* reporter assay (Figure 2). The H60C and H67C mutant RcnR proteins show significant depression of P_{rcnA} transcription in response to Ni(II) or Co(II) addition. The H64C mutation was tested for metal responsiveness to Ni(II), Co(II), Cu(II) and Zn(II) (Figure 2); Cu(II) ions will be reduced to Cu(I) in the cytoplasm of the cell), as well as Cd(II) (Supporting Information Figure S2) (40). Only in the presence of Co(II) was the H64C-RcnR mutant protein able to de-repress P_{rcnA} transcription. Although several mutants have been previously characterized by Iwig *et al.* (24) that show a significant response to Ni(II) binding but not to Co(II) binding, this is the first mutant characterized to date that shows a significant response to binding Co(II) over binding Ni(II), and is further evidence that the two cognate metals are recognized by distinct mechanisms.

XANES analysis of H60C-, H64C- and H67C-RcnR

Information regarding the coordination number and geometry of a metal center can be obtained by analyzing the XANES spectrum. XANES for H60C-, H64C- and H67C-RcnR metal complexes are summarized in Table 1 and shown in Figure 3. Metals with a vacancy in the 3d manifold (*e.g.,* Co(II) and Ni(II)) exhibit features in the XANES associated with bound transitions below the edge energy. These features include the 1s→3d transition (with shake-down contributions) which is a measure of centrosymmetricity in the complex, and the peak associated with a $1s\rightarrow 4p_z$ transition, which is present in tetragonal geometries lacking one or more axial ligand.

The Co(II) complexes of H60C-, H64C- and H67C-RcnR proteins have a single pre-edge feature at ~7710 eV (Table 1, Figure 3) that is associated with the 1s→3d transition. Like

NIH-PA Author Manuscript

NIH-PA Author Manuscript

NIH-PA Author Manuscript

the WT protein (24), the peak areas observed for the Co(II) protein complexes are larger than that typical octahedral Co(II) complexes (0.069(8) eV) (28) but smaller than that observed for five-coordinate complexes (0.220(3) eV) (29). The larger 1s→3d peak areas observed for these Co(II) RcnR mutant protein complexes is consistent with a distorted octahedral geometry (41). The Ni(II) complexes of H60C-, H64C- and, H67C-RcnR all have a relatively small peak associated with the 1s→3d transition located at ~8330 eV (Table 1, Figure 3) suggesting that the ligand arrangements are centrosymmetric (42). Only the spectrum obtained for H64C-RcnR + Ni(II) exhibits a small shoulder at ~8338 eV, which corresponds to a 1s→4p_z transition, consistent with either a distorted square planar geometry or square-pyramidal geometry (42). The presence of this small shoulder coupled with the small 1s→3d peak area (0.016 eV) is most consistent with a distorted square-planar geometry (42). The rest are therefore determined to be six-coordinate.

Cu(I) and Zn(II) complexes have no 1s→3d transitions as they are d^{10} metals. For the Cu(I) complexes there is a well resolved 1s→4p transition between 8983 and 8985 eV (43). The shape, energy and intensity of this peak can be used to determine the coordination geometry of the Cu(I) metal center (43). The 1s→4p transition in 2-, 3- and 4-coordinate model complexes have normalized absorption magnitudes of ~1, ~0.55 and between 0.6 and 0.9 at ~8994, 8994 and 8995.5 eV respectively (43). H60C-, H64C-, H67C- and WT-RcnR (25) Cu(I) complexes have a normalized intensity of 0.49, 0.48, 0.49 and 0.46 respectively at ~8984 eV. The intensity and the energy of this peak suggest that the Cu(I) complexes are three-coordinate.

For Zn(II) complexes, information can be gained about the coordination number and geometry from intensity and shape of the XANES spectra (44, 45). Information regarding the coordination number of the Zn(II) center can be determined by the intensity of the XANES as well as the relative position of the edge in energy (45). The normalized intensity of what is termed the white line, the sharp intense peak arising from the absorption edge, feature increases with increasing coordination number. For four-coordinate complexes the normalized intensity of the white line is ~1.3, five- and six-coordinate complexes have an intensity between 1.3 and 2, with six-coordinate being the most intense (45). The edge energy for six-coordinate complexes is ~2 eV higher than that of four- or five-coordinate complexes (45). The XANES spectra for the WT Zn(II) complex is consistent with a four-coordinate complex (25), whereas the edge energies and intensities of the Zn(II) complexes of the H60C-, H64C- and H67C-RcnR in buffer M with 300 mM NaBr are consistent with six coordinate complexes for all three mutations. The corresponding Zn(II) complexes in buffer M with 300 mM NaOAc have edge energies that are more consistent with four/five coordinate Zn(II) complexes (~9663 eV) (45).

EXAFS analysis of H60C-, H64C- and H67C-RcnR Complexes

EXAFS analysis provides information regarding the atomic number of scattering atoms (Z ± 2), the distance between the absorbing and scattering atom (± 0.02 Å in the first coordination sphere), and an estimate of the number of similar and distinct ligands (± ~20% for the total number of ligands).

H60C-RcnR

Table 1 and Figure 4 show the best fits for metal complexes of H60C-RcnR proteins in buffer M containing NaBr as well as the Zn(II) complex in buffer M with NaOAc. The best fits for the cognate metals, Ni(II) and Co(II) are six-coordinate in agreement with the XANES analysis (*vide supra*), and the ligand environment is composed of 5N/O- and 1S-donor ligands, as is the case for the WT protein (24, 25). Neither cognate metal picks up a second S-donor ligand, nor do they bind anions (*e.g.,* Br^-) from the buffer, suggesting that

NIH-PA Author Manuscript

NIH-PA Author Manuscript

NIH-PA Author Manuscript

like WT-RcnR, all six ligands are derived from the protein (24, 25). The Ni(II) site structure in H60C-RcnR is essentially unaltered from the WT Ni(II) site structure, as both feature a long ~2.61(2) Å Ni-S distance and 1–2 His imidazole ligands among five N/O-donors with Ni-L distances of ~2.1 Å. These results are consistent with the His60 sidechain not being a ligand in the WT-RcnR Ni(II) complex.

The Co(II) site fits best for two or three imidazole ligands; the tendency for increased His ligation in the Co(II) complex relative to the Ni(II) complex is similar to that seen in the WT protein (25). However, the Co(II) site in H60C-RcnR has a long 2.6 Å Co-S distance that is significantly altered from the Co(II) site in WT-RcnR (2.3 Å), and more closely resembles the Ni(II) site in WT-RcnR in this respect (24, 25). Although the data cannot unambiguously differentiate Cys35 from Cys60 as the source of the S-donor ligand, the fact that Co(II), Ni(II), Cu(I) and Zn(II) ions all bind to Cys35 in the WT protein (25), and other mutants have been characterized where the Co(II) site features a the long M-S distance (*e.g.,* H3C-RcnR, H3E-RcnR) (25) is consistent with the S-donor present being Cys35. Nonetheless, it is not clear whether the structure changed because of the loss of His60 as a ligand, or as the result of another structural change in the metal site (*e.g.,* loss of an H-bond) that results in Co(II) occupying a site that more closely resembles the WT-RcnR Ni(II) site. Since one might expect that the mutation would result in the loss of one His ligand and feature two Cys S-donors if His60 were a Co(II) ligand, the result is more consistent with a role for His60 as a secondary coordination sphere residue involved in stabilizing the WT Co(II) conformation of the protein. The *lacZ* assay data (*vide supra*) show that the protein is still responsive to both Co(II) and Ni(II) binding. This is probably due to the fact that both metals adopt a geometry and a ligand set that is similar to that of Ni(II) binding to WT-RcnR, and therefore supports a role for His60 in stabilizing the Co(II) conformation as seen in the Co(II) WT complex (24).

The structures of the non-cognate metal ions, Cu(I) and Zn(II) show dramatically different responses to the H60C-RcnR mutation. A four-coordinate Cu(I) complex forms with H60C-RcnR that is composed of a $(N/O)_2SBr$ ligand donor atom set that incorporates a bromide from the buffer. Like the Co(II) and Ni(II) complexes of H60C-RcnR, the metal does not bind to two S-donors. The ligands involved in the Cu(I) H60C-RcnR complex are identical to those seen for the Cu(I) complex of WT-RcnR; the M-L distances are similar (for WT-RcnR: Cu - N = 2.13(2) Å; Cu – S = 2.291(7) Å; Cu – Br = 2.62(1) Å) (25). The similarity of these structures indicates that His60 is not a ligand involved in Cu(I) binding to WT-RcnR. According to the EXAFS analysis, the coordination number of the Cu(I) center is four, a result that is inconsistent with the XANES analysis (*vide supra*) that predicts a three-coordinate Cu(I) site (Table 1, Figure 3). A similar discrepancy is observed in the analysis of data from the WT-RcnR Cu(I) complex (25). It is possible that the long (weak) interactions with Br^- are not enough to alter the XANES features to indicate a four-coordinate site.

In contrast to the Ni(II), Co(II) and Cu(I) complexes of H60C-RcnR, the best fit for the Zn(II) H60C-RcnR complex shows that both Cys residues are ligands. Additionally, the data obtained for the Zn(II) site indicates that the Zn(II) is coordinated by three N/O-donors, of which 2 - 3 are imidazoles, and a bromide ligand, making the complex six-coordinate, in agreement with the XANES analysis (*vide supra*). This contrasts with the four-coordinate tetrahedral $Zn[(N/O)_2SBr]$ complex found for the WT-RcnR Zn(II) complex (25). Although six-coordinate Zn(II) sites are unusual (46), they are not unprecedented in RcnR mutants. In a series of His3 mutations, H3L has no effect on the Zn(II) site, the H3C mutation results in a five-coordinate $Zn[(N/O)_2S_2Br]$ that becomes a six- or seven-coordinate (with a bidentate carboxylate) $Zn[(N/O)_6S]$ site in H3E-RcnR, and confers Zn-sensing capability to the protein (25). Although His3 is clearly not a ligand for the WT-RcnR Zn(II) site, the site displays an ability to accommodate additional ligands and to change coordination number.

NIH-PA Author Manuscript

NIH-PA Author Manuscript

NIH-PA Author Manuscript

The coordination number of the Zn(II) complexes of H60C-RcnR also shows some unusual sensitivity to the nature of the anions present in the buffer. The Zn(II) complex of H60C-RcnR is six-coordinate in buffer M with NaBr, but five-coordinate in buffer M with NaOAc (Table 1). The Zn(II) H60C-RcnR in buffer M with NaBr fits best for three N/O-donors at an average distance of 2.00 Å of which two to three are imidazoles, two S-donor at 2.35 Å and a Br^--ligand at 2.33 Å. The bond lengths determined for the Zn-S and the Zn-Br bonds are almost indistinguishable. For this reason, the data were also taken in buffer M with NaOAc. The EXAFS data from Zn(II) H60C-protein in buffer M with NaOAc (Figure 4) fit best for three N/O donors at 2.04 Å, of which one to two are imidazoles, and two S-donors at 2.30 Å. The sample in NaOAc buffer yielded a similar fit sans the Br^--ligand, confirming that the protein did, in fact, bind both sulfurs present in the H60C protein.

H64C-RcnR

The His64 residue of RcnR corresponds to a cysteine residue in *M. tuberculosis* CsoR, Cys65 (Figure 1), and this cysteine residue is a key ligand used to coordinate Cu(I) in CsoR (17). The Co(II) complex of H64C RcnR is shown by XANES analysis to be six-coordinate, and EXAFS analysis is consistent with this. The EXAFS shows more than one change in metal site structure occurs for this mutation. The Co(II) site is composed of three N/O-donors, of which two to three are histidines, at an average distance of 2.02 Å, two S-donors at an average distance of 2.33 Å and one Br^- ligand at 2.67 Å (Table 1 and Figure 5). The fit is similar in buffer with NaCl except that a Cl^- ligand is bound instead of a Br^- (Supporting Information, Table S10). This mutation resulted in binding the Cys64 residue, which is consistent with His64 being a ligand in the WT-RcnR Co(II) complex, but also opened a coordination site on Co(II) that is occupied by an exogenous buffer ligand. The analysis cannot identify the N/O-donor ligand that is lost, and the reason for the loss is not clear. However, changing a protein ligand from an imidazole to a thiolate will affect the electronic structure of the metal, which can influence the strength of interaction with other ligands.

In contrast to the Co(II) site in H64C RcnR, the best fit for the Ni(II) EXAFS data is five-coordinate with three histidine ligands at an average distance of 2.05 Å, one S-donor at 2.31 Å and a Brat 2.69 Å (Table 1 and Figure 5). [There is also a four-coordinate fit that is similar with the exception that there is one less histidine ligand and the Ni-S bond distance is shorter, consistent with a four-coordinate nickel center (47). However, the five-coordinate fit improves both %R and reduced χ^2 by 40%. A similar result was observed for this sample in buffer with NaCl (Supporting Information, Table S12), where the five-coordinate EXAFS fit improves %R and reduced χ^2 by 12% (Supporting Information, Table S12).] Whether the site has a distorted four- or five-coordinate geometry, the data show a major disruption of the WT-RcnR Ni(II) site structure that is at least consistent with the involvement of His64 as a Ni(II) ligand. The structure obtained for the mutant protein involves a short Ni-S bond that is comparable to the Co – S distance that is found in WT-RcnR (24, 25), but it is not clear which of the two Cys residues is involved, particularly given the large number of structural changes involved.

The complexes formed with H64C-RcnR and non-cognate metal ions, Cu(I) and Zn(II) are similar to those formed by the H60C mutation, suggesting that His64 may be a ligand of Zn(II), but is clearly not a ligand for Cu(I). EXAFS analysis for the Cu(I) sample reveals that the Cu(I) site is four coordinate and binds the exogenous buffer ligand similar to that seen for Cu(I) H60C-RcnR and in WT-RcnR (25). However, Cu(I) H64C-RcnR in buffer with NaCl (Supporting Information, Table S14) indicates that the best fit for the data is three-coordinate with two N/O-donors at 2.10 Å and one S-donor at 2.36 Å. The appearance of Br^-, but not Cl^-, in the coordination sphere of Cu(I) was also noted in the WT-RcnR Cu(I) complex (25), and is not surprising considering the facts that Cu(I) often occupies

NIH-PA Author Manuscript

NIH-PA Author Manuscript

NIH-PA Author Manuscript

three-coordinate sites and is also a softer acid, and would thus have a higher affinity for Br^- than for Cl^-.

Like the Zn(II) H60C-RcnR protein, the Zn(II) site in the H64C-RcnR protein is also six-coordinate in buffer M with NaBr and five-coordinate in buffer with NaOAc (Table 1). The difference between the two fits being that the sample in buffer M with NaBr has an additional Br^--ligand derived from the buffer. The Zn(II) H64C-RcnR complex formed in buffer M with NaBr is coordinated by three N/O-ligands at an average distance of 2.05 Å, of which two to three are imidazoles, two S-donors at 2.40 Å and a Br^--ligand at 2.36 Å.

H67C-RcnR

The XANES and EXAFS analysis are in agreement for the cognate metals, which feature six-coordinate sites (Table 1). Like H60C-RcnR, the Co(II) site resembles that of the Ni(II) site in that the Co(II) metal ion is coordinated by a S-donor ligand at 2.63 Å. The best fit for the Co(II) site is for two shells of N/O-donors, three at an average distance of 2.07 Å and two at an average distance of 2.20 Å, of which two to three are imidazoles, and a S-donor at 2.63 Å (Table 1, Figure 6). The Ni(II) site fits best for five N/O-donors at an average distance of 2.06 Å, of which two are imidazoles, and a S-donor at 2.62 Å. The corresponding fit involving three imidazoles results in an improvement in both %R and reduced χ^2, however the error for the sulfur bond distance is larger, and for this reason the sample was repeated in buffer M containing NaOAc. The best fit for this data is five N/O-donors, of which two are imidazoles, and a S-donor ligand, a result that is indistinguishable from the WT-RcnR Ni(II) site structure (25).

The Cu(I) site in H67C-RcnR is three-coordinate, in agreement with the XANES analysis. The site is coordinated by a histidine ligand at 2.04 Å, a S-donor at 2.31 Å and a Br^- at 2.51 Å. The Cu(I) is still coordinated by an exogenous buffer ligand but differs from the H60C-, and H64C-RcnR Cu(I) samples in that it binds one less N/O-donor. Thus, His67 is either a ligand of the Cu(I) complex or necessary for the positioning of another amino acid side chain to coordinate Cu(I). The Zn(II) site shows some variability based on buffer selection. The sample in buffer with NaBr (Table 1, Figure 6) is a six-coordinate $Zn[(N/O)_5S]$ site, with a Zn-S distance of 2.27 Å. As such, it resembles the WT-RcnR Co(II) site structure. However, in buffer containing NaOAc the Zn(II) ion adopts a four-coordinate $Zn[(N/O)_2S_2]$ structure that coordinates both Cys residues present in the protein, consistent with H67 being a ligand in the four-coordinate site. This is the fourth example of the coordination number of a metal site in an RcnR protein being influenced by the nature of the anion bound, and the first example of an alteration in the protein ligand selection by the metal center. For Cu(I), the metal is often four-coordinate with bromide present, but is three coordinate in alternate buffers, without an obvious alteration in the remaining three ligands.

Discussion

Metalloregulator function depends upon a selective response to binding by a cognate metal ion. Selectivity is generally elicited by requiring a coordination geometry that is favored by the cognate metal and disfavored by non-cognate metals. The ramifications of the RcnR His to Cys mutations to metal site structures provide further insight into the role of specific His ligands in complexes formed with cognate and non-cognate metal ions, and show that in some cases, a Co(II) response may be observed when the Co(II) ion adopts a structure similar to the WT-RcnR Ni(II) site.

NIH-PA Author Manuscript

NIH-PA Author Manuscript

NIH-PA Author Manuscript

Cognate metal complexes

The results presented here, along with those obtained previously (24, 25) collectively suggest that His3, His60 and His64 and His67 are potential Co(II) ligands. Histidine coordination appears to be less important for Ni(II) binding, as only His64 has been clearly shown to be important for the six-coordinate Ni(II) site. The precise roles of His60 and His67 in the Co(II)–WT-RcnR complex are obscured by the fact that the H60C and H67C mutations lead to Co(II) site structures that resemble the WT-RcnR Ni(II) complex (24, 25) and do not introduce an additional S-ligand. Thus, it is possible that His60 and His67 play allosteric roles that stabilize a unique protein structure that gives rise to the WT-RcnR Co(II) complex. Alternatively, because the mutation affects the chemical identity of the side chain, the potential for main chain coordination cannot currently be excluded. These results are in general agreement with those from a mutational survey by Iwig *et al.* (24), based on the loss of transcriptional response in *lacZ* reporter assays. Those studies showed that His3 and His64 are important for response to both Ni(II) and Co(II) bound to WT-RcnR, and His60 mutations impair only the Co(II) response (24). His3 was later shown using XAS to be a ligand in the Co(II) complex, but not in the Ni(II) complex, suggesting an allosteric role for His3 in the Ni(II) complex (25).

Functional studies carried out by Iwig *et al.*(24) showed that when His60 was mutated to Ala, Asn, Leu and Arg, all of the mutations resulted in a loss of Co(II) responsive transcriptional regulation by RcnR. However, only H60R-RcnR resulted in a loss of responsiveness for both cognate metals (Ni(II) and Co(II)), with the remaining mutations resulting in proteins that were still Ni(II) responsive, demonstrating that the His60 sidechain was not essential for response to Ni(II)-specific function. For the H60C mutation studied here, RcnR retains a response to *both* cognate metals. However, the structural information available from XAS analysis shows that this is not due simply to the swap of one protein ligand (His) for another (Cys), since neither cognate metal ion coordinates an additional S-donor ligand. The structure of the Ni(II) site is not perturbed by the mutation, indicating that His60 is not a ligand in the Ni(II) site, and in agreement with expectations from the prior mutagenesis studies (24). However, the Co(II) site structure is altered in H60C-RcnR. Although it also does not show ligation of both Cys residues, the structure features the long Co-S distance that is reminiscent of the M-S distance seen in the WT-RcnR Ni(II) site (24, 25), but not in the WT-RcnR Co(II) site. Based on studies of the N-terminus of the protein that showed that differential recognition of Co(II) vs. Ni(II) involved His3 as a ligand only in the Co(II) case, as well as the different M-S distances, a model that involved different protein conformations in the two complexes was developed to explain differential recognition of Co(II) and Ni(II). Other mutants involving His3 were found to bind Co(II), but with metric parameters that closely resembled the WT-RcnR Ni(II) site (25). Many of these mutants had residual responses to Co(II) ions. The H60C-RcnR mutant protein may be responsive to Co(II) because it is recognizing the ion by the same mechanism that WT-RcnR recognizes Ni(II).

When His64 was mutated to Leu, it eliminated Co(II) response but only slightly impaired Ni(II) responsiveness (24), suggesting a similar scenario to that described above for the His60 mutations. However, the H64C mutation results in the first example of an RcnR protein that retains a significant response to Co(II) but lacks a response to binding Ni(II) (Figure 2). The XAS studies show that the H64C-RcnR Co(II) site resembles the Co(II) site in WT-RcnR (25) with substitution of a His64 ligand by the additional Cys ligand, including maintenance of the 2.3 Å Co-S distance. This is the result expected for a simple ligand substitution, producing a protein that is able to maintain the six-coordinate structure of the WT-RcnR complex, and thus its response to Co(II) binding. Therefore, His64 may play a similar role in Co(II) binding in RcnR as His86 and His100 in the Zn(II) responsive transcriptional regulator in *S. aureus* CzrA. CzrA binds Zn(II) in a tetrahedral geometry with

NIH-PA Author Manuscript

NIH-PA Author Manuscript

NIH-PA Author Manuscript

three histidines and one aspartate (His86, His97, His100 and Asp84) (48). Mutagenesis studies coupled with DNA binding and UV-vis studies (using the Co(II) protein) revealed that Asp84 and His97 are necessary to maintain tetrahedral geometry and Zn(II) mediated regulation. Mutations of these residues resulted in metal binding in non-native geometries that did not support allosteric coupling of metal and DNA binding (49). However, His86 and His100 are necessary for Zn(II) binding, but metal binding residues like Asp, Glu, Asn and Gln were shown to coordinate Zn(II) in a tetrahedral environment and mediate DNA binding (49). Like His86 and His100 in CzrA, His64 in RcnR is necessary for Co(II) binding and mutating His64 to another metal binding residue such as Cys maintains an octahedral geometry for the Co(II) site necessary for mediating the regulation of RcnR binding to DNA.

In the case of Ni(II), the H64C-RcnR binding site is disrupted in the complex in a way that does not maintain the Ni-S distance in the WT-RcnR structure, does not incorporate a second Cys ligand, and opens the site to exogenous anion binding. This mutation changes the Ni(II) site from six-coordinate in the case of WT-RcnR (24, 25) to four-/five-coordinate with the loss of at least two protein ligands and the addition of an exogenous buffer ligand, suggesting that His64, like the N-terminus (25), is necessary for maintaining a six-coordinate Ni(II) site. The H64C mutation results in a loss of Ni(II) response, but provides no further insight into the role of His64 as a Ni(II) ligand, which could be part of an allosteric network that maintains the conformation of the protein in the Ni(II) complex.

Finally, His67 has also been previously mutated to Leu, which had no effect on responsiveness to either of the cognate metals. This result is also seen for the H67C-RcnR mutation reported here. However, XAS structural analysis shows that the Co(II) ion adopts a structure similar to the WT-RcnR Ni(II) site structure (M-S ~ 2.6 Å) (25), indicating that the Co(II) response is being maintained in H67C-RcnR by the mechanism used to generate a response to Ni(II) binding. Although the results do not prove a role for His67 as a Co(II) ligand, His67 must at least play a role in stabilizing the Co(II) site structure in WT-RcnR, either as a ligand or through H-bonding interactions that stabilize the protein structure. His67 is not conserved in RcnR proteins and is predicted to be in a loop region, based on structural homology with CsoR.

Non-cognate metal complexes

The effect of the His60, His64, and His67 residues on the structures of the non-cognate metal ions reveals that these residues have distinctive roles in binding non-cognate metals. These sites overlap with the cognate metal binding sites, for example in the use of Cys35 as a ligand, but in some cases His ligands that are involved in binding non-cognate metals are not involved in binding the cognate metals. This suggests that the sites occupied by non-cognate metals may prevent these metals from binding to some of the ligands adopted by cognate metals (*e.g.,* the N-terminal amine).

Cu(I)

The Cu(I) complexes with the His → Cys mutants are either three- or four- coordinate, depending upon whether a buffer anion is bound. Even with the additional Cys residue added by the H60C-, H64C-, and H67C-RcnR mutant proteins the Cu(I) site does not resemble that of Cu(I)-bound CsoR, which has a coordination environment involving one His ligand and two S-donors (17). The Cu(I) complex of H60C-RcnR has a structure that is very much like Cu(I) WT-RcnR (25), and does not bind the second Cys residue available in this mutant. Thus, His60 is likely not a ligand for Cu(I)-RcnR. Similarly, the Cu(I) site in H64C-RcnR is unaffected by the mutation and is similar to that seen for the Cu(I) complex of WT-RcnR (25) and H60C-RcnR. The complex formed by Cu(I) and H67C-RcnR is

NIH-PA Author Manuscript

NIH-PA Author Manuscript

NIH-PA Author Manuscript

distinct from the H60C and H64C mutants. The coordination number drops from four-coordinate in the other mutants (including bromide), to three-coordinate with the loss of one His ligand. Thus, His67 is identified as a ligand for Cu(I). Based on the $His_2(Cys)Br$ ligand set seen in the Cu(I) WT-RcnR complex in buffer M with NaBr (25), the only ligand in common with the WT-RcnR Ni(II) site is the single Cys35 ligand. Interestingly, Cu(I) never bound a $His(Cys)_2$ ligand set like found in Cu(I)-CsoR, even when presented with the identical CsoR ligand set in H64C-RcnR.

Zn(II)

The situation for Zn(II) is more complex. In buffer M containing NaBr, all three His → Cys mutants are six-coordinate and therefore presumably occupy a six-coordinate site that is more similar to the WT-RcnR Co(II) and Ni(II) sites than to the WT Zn(II) site. The cognate metals both utilize His64, and Co(II) may also bind to His60 (*vide supra*). The Zn(II) complexes of H60C- and H64C-RcnR show the formation of a six-coordinate $(N/O)_3S_2Br$ complex in buffer M with NaBr, consistent with these residues being ligands in the six-coordinate site. The Zn-S distance is 2.40 Å, and so the site most closely resembles the WT-RcnR Co(II) site, and is very similar to the $(N/O)_3S_2Br$ Co(II) site in the H64C-RcnR mutant. In buffer M with NaOAc, the bromide ligands are not present and five-coordinate $(N/O)_3S_2$ complexes are observed.

The complex formed by H67C-RcnR with Zn(II) is distinct from the other His mutants. In buffer M with NaBr, the $(N/O)_5S$ complex formed is six-coordinate, but features only a single S-donor and has no bromide ligand. The Zn-S distance is long (2.69(4) Å), and thus this site most closely resembles the WT-RcnR Ni(II) site. However, in buffer M with NaOAc, Zn(II) adopts a four-coordinate $(N/O)_2S_2$ site, where Cys67 is a ligand, consistent with His67 being a ligand in the four-coordinate WT-RcnR Zn(II) site. However, this possibility cannot be distinguished from simple displacement of the bromide ligand found in the WT-RcnR $(N/O)_2SBr$ site by the additional cysteinate ligand.

Distinct mechanisms for metal recognition by orthologs RcnR and CsoR

The results of this and previous studies (24, 25) indicate that besides coordination number and ligand selection, there is a key difference between the molecular mechanisms that couple metal recognition to allosteric response in the RcnR/CsoR family of transcriptional regulators. Only two of the Cu(I) binding residues in CsoR are conserved in RcnR; Cys36 and His61 (using *M. tuberculosis* CsoR numbering). Additionally, in RcnR proteins, there is a conserved His residue at position 3. This residue corresponds to Glu4 in *M. tuberculosis* CsoR. Based on the *M. tuberculosis* CsoR crystal structure, Glu4 is positioned close to the CsoR Cu(I) binding site (17). Prior studies of RcnR have established that cognate metal binding to the N-terminal amine as well as the interaction with His3 are key determinants in the mechanism of metal recognition by RcnR that apparently play no role in CsoR Cu(I) binding (24, 25).

None of the RcnR His → Cys mutants studied here confer any response to either Cu(I) or Zn(II), including H64C-RcnR, where the residues are identical to those in the Cu(I) binding site of CsoR, or adopt the Cu(I) site structure found in that protein. As seen in InrS (23) simply having the first coordination sphere residues present necessary for Cu(I) binding (as seen in CsoR) is not sufficient to elicit Cu(I) responsiveness (17, 50). The Cu(I)-CsoR structure reveals that there is a hydrogen-bonding network involving metal-binding residue His61 as well as Tyr35 and Glu81. Work done by Ma *et al.* determined that this hydrogen-bonding network is important in allosterically coupling metal-binding with DNA-binding in CsoR (50). Even if Cu(I) were to bind H64C RcnR with $His(Cys)_2$ coordination, as in CsoR, it is likely the protein would not show a change in DNA-binding affinity because the protein

NIH-PA Author Manuscript

NIH-PA Author Manuscript

NIH-PA Author Manuscript

lacks the second coordination sphere residues needed to couple metal-binding with DNA-binding (17, 50). This data indicates that while the secondary, tertiary and quaternary structures of CsoR and RcnR are similar, the specific mechanisms for metal ion recognition are quite different and small changes in primary sequence account for changes not just in coordination geometry but also in the allosteric network of residues required for a functional response.

The Zn(II) H60C-, H64C- and H67C-RcnR mutants all feature six-coordinate Zn(II) sites. However, Zn(II) binding to these mutant proteins does not result in the derepression of P_{rcnA} transcription. Thus, the mere formation of a six-coordinate Zn(II) site is not sufficient to provide a transcriptional response, despite the one observed for the Zn(II) complex of H3E-RcnR (25). Although Zn(II) adopts the correct geometry in the H60C-, H64C- and H67C-RcnR mutations, they apparently do not allow the Zn(II) ion to bind the N-terminus of RcnR and therefore cannot drive the necessary conformational changes required to disfavor RcnR-DNA binding interactions.

The identification of Cu(I) and Zn(II) coordinating residues in RcnR, combined with the different allosteric networks utilized by RcnR and CsoR, suggests that the metal-specificity of RcnR could be reengineered via judicious mutations that promote Cu(I) or Zn(II) binding but not Ni(II) or Co(II) binding. Additional directed mutations in the N-terminus of RcnR would be required to ensure binding produces a functional response. This has already been observed in Zn(II)-substituted H3E-RcnR (25), which offers promise for additional successful engineering.

Supplementary Material

Refer to Web version on PubMed Central for supplementary material.

List of Abbreviations

Amp	Ampicillin
Cam	Chloramphenicol
CsoR	Copper-sensitive operon repressor
E. coli	*Escherichia coli*
EPR	Electron paramagnetic resonance
EXAFS	Extended x-ray absorption fine structure
Hyp	Hydrogenase pleiotropy
H_2ase	Hydrogenase
InrS	Internal nickel-responsive sensor
ICP-OES	Inductively coupled plasma-optical emission spectroscopy
IPTG	Isopropyl β-D-1-thiogalactopyranoside
M. tuberculosis	*Mycobacterium tuberculosis*
NikR	Nickel responsive regulator of the *nik* operon
RcnR	Resistance to cobalt and nickel repressor
S. lividans	*Streptomyces lividans*
TCEP	Tris(2-carboxyethyl)-phosphine hydrochloride

NIH-PA Author Manuscript

NIH-PA Author Manuscript

NIH-PA Author Manuscript

T. thermophilus	*Thermus thermophilus*
XANES	X-ray absorption near edge spectroscopy
XAS	X-ray absorption spectroscopy

References

1. Rosenzweig AC. Metallochaperones: bind and deliver. Chem Biol. 2002; 9:673–677. [PubMed: 12079778]
2. Pennella MA, Giedroc DP. Structural determinants of metal selectivity in prokaryotic metal-responsive transcriptional regulators. BioMetals. 2005; 18:413–428. [PubMed: 16158234]
3. Böck A, King PW, Blokesch M, Posewitz MC. Maturation of hydrogenases. Adv Microb Physiol. 2006; 51:1–71. [PubMed: 17091562]
4. Forzi L, Sawers RG. Maturation of [NiFe]-hydrogenases in *Escherichia coli*. BioMetals. 2007; 20:565–578. [PubMed: 17216401]
5. De Pina K, Navarro C, McWalter L, Boxer DH, Price NC, Kelly SM, Mandrand-Berthelot MA, Wu LF. Purification and characterization of the periplasmic nickel-binding protein NikA of *Escherichia coli* K12. Eur J Biochem. 1995; 227:857–865. [PubMed: 7867647]
6. Navarro C, Wu LF, Mandrand-Berthelot MA. The nik operon of *Escherichia coli* encodes a periplasmic binding-protein-dependent transport system for nickel. Mol Microbiol. 1993; 9:1181–1191. [PubMed: 7934931]
7. Atanassova A, Zamble DB. *Escherichia coli* HypA is a zinc metalloprotein with a weak affinity for nickel. J Bacteriol. 2005; 187:4689–4697. [PubMed: 15995183]
8. Mehta N, Olson JW, Maier RJ. Characterization of *Helicobacter pylori* nickel metabolism accessory proteins needed for maturation of both urease and hydrogenase. J Bacteriol. 2003; 185:726–734. [PubMed: 12533448]
9. Zhang JW, Butland G, Greenblatt JF, Emili A, Zamble DB. A role for SlyD in the Escherichia coli hydrogenase biosynthetic pathway. J Biol Chem. 2005; 280:4360–4366. [PubMed: 15569666]
10. Leach MR, Sandal S, Sun H, Zamble DB. Metal binding activity of the *Escherichia coli* hydrogenase maturation factor HypB. Biochemistry. 2005; 44:12229–12238. [PubMed: 16142921]
11. Rodrigue A, Effantin G, Mandrand-Berthelot MA. Identification of rcnA (yohM), a nickel and cobalt resistance gene in *Escherichia coli*. J Bacteriol. 2005; 187:2912–2916. [PubMed: 15805538]
12. Koch D, Nies DH, Grass G. The RcnRA (YohLM) system of *Escherichia coli*: a connection between nickel, cobalt and iron homeostasis. BioMetals. 2007; 20:759–771. [PubMed: 17120142]
13. Blériot C, Effantin G, Lagarde F, Mandrand-Berthelot MA, Rodrigue A. RcnB is a periplasmic protein essential for maintaining intracellular Ni and Co concentrations in *Escherichia coli*. J Bacteriol. 2011; 193:3785–3793. [PubMed: 21665978]
14. De Pina K, Desjardin V, Mandrand-Berthelot MA, Giordano G, Wu LF. Isolation and characterization of the nikR gene encoding a nickel-responsive regulator in *Escherichia coli*. J Bacteriol. 1999; 181:670–674. [PubMed: 9882686]
15. Chivers PT, Sauer RT. NikR is a ribbon-helix-helix DNA-binding protein. Protein Sci. 1999; 8:2494–2500. [PubMed: 10595554]
16. Iwig JS, Rowe JL, Chivers PT. Nickel homeostasis in *Escherichia coli* - the rcnR-rcnA efflux pathway and its linkage to NikR function. Mol Microbiol. 2006; 62:252–262. [PubMed: 16956381]
17. Liu T, Ramesh A, Ma Z, Ward SK, Zhang L, George GN, Talaat AM, Sacchettini JC, Giedroc DP. CsoR is a novel *Mycobacterium tuberculosis* copper-sensing transcriptional regulator. Nat Chem Biol. 2007; 3:60–68. [PubMed: 17143269]
18. Ma Z, Jacobsen FE, Giedroc DP. Coordination chemistry of bacterial metal transport and sensing. Chem Rev. 2009; 109:4644–4681. [PubMed: 19788177]
19. Iwig JS, Chivers PT. DNA recognition and wrapping by *Escherichia coli* RcnR. J Mol Biol. 2009; 393:514–526. [PubMed: 19703465]

NIH-PA Author Manuscript NIH-PA Author Manuscript NIH-PA Author Manuscript

20. Blaha D, Arous S, Bleriot C, Dorel C, Mandrand-Berthelot MA, Rodrigue A. The *Escherichia coli* metallo-regulator RcnR represses rcnA and rcnR transcription through binding on a shared operator site: Insights into regulatory specificity towards nickel and cobalt. Biochimie. 2011; 93:434–439. [PubMed: 21040754]
21. Sakamoto K, Agari Y, Agari K, Kuramitsu S, Shinkai A. Structural and functional characterization of the transcriptional repressor CsoR from *Thermus thermophilus* HB8. Microbiology. 2010; 156:1993–2005. [PubMed: 20395270]
22. Dwarakanath S, Chaplin AK, Hough MA, Rigali S, Vijgenboom E, Worrall JA. Response to Copper Stress in *Streptomyces lividans* Extends beyond Genes under Direct Control of a Copper-sensitive Operon Repressor Protein (CsoR). J Biol Chem. 2012; 287:17833–17847. [PubMed: 22451651]
23. Foster AW, Patterson CJ, Pernil R, Hess CR, Robinson NJ. Cytosolic Ni(II) sensor in cyanobacterium: Nickel detection follows nickel affinity across four families of metal sensors. J Biol Chem. 2012; 287:12142–12151. [PubMed: 22356910]
24. Iwig JS, Leitch S, Herbst RW, Maroney MJ, Chivers PT. Ni(II) and Co(II) sensing by *Escherichia coli* RcnR. J Am Chem Soc. 2008; 130:7592–7606. [PubMed: 18505253]
25. Higgins KA, Chivers PT, Maroney MJ. Role of the N-terminus in determining metal-specific responses in the *E. coli* Ni- and Co-responsive metalloregulator, RcnR. J Am Chem Soc. 2012; 134:7081–7093. [PubMed: 22471551]
26. Ma Z, Cowart DM, Scott RA, Giedroc DP. Molecular insights into the metal selectivity of the copper(I)-sensing repressor CsoR from *Bacillus subtilis*. Biochemistry. 2009; 48:3325–3334. [PubMed: 19249860]
27. Thompson JD, Higgins DG, Gibson TJ. CLUSTAL W: improving the sensitivity of progressive multiple sequence alignment through sequence weighting, position-specific gap penalties and weight matrix choice. Nucleic Acids Res. 1994; 22:4673–4680. [PubMed: 7984417]
28. Leitch S, Bradley MJ, Rowe JL, Chivers PT, Maroney MJ. Nickel-specific response in the transcriptional regulator, *Escherichia coli* NikR. J Am Chem Soc. 2007; 129:5085–5095. [PubMed: 17397155]
29. Padden KM, Krebs JF, MacBeth CE, Scarrow RC, Borovik AS. Immobilized metal complexes in porous organic hosts: development of a material for the selective and reversible binding of nitric oxide. J Am Chem Soc. 2001; 123:1072–1079. [PubMed: 11456660]
30. Webb SM. SIXpack: A graphical user interface for XAS analysis using IFEFFIT. Phys Scr. 2005; T115:1011–1014.
31. Ankudinov AL, Ravel B, Rehr JJ, Conradson SD. Real-space multiple-scattering calculation and interpretation of x-ray-absorption near-edge structure. Phys Rev B. 1998; 58:7565–7576.
32. Zabinsky SI, Rehr JJ, Ankudinov A, Albers RC, Eller MJ. Multiple-scattering calculations of x-ray-absorption spectra. Phys Rev B: Condens Matter. 1995; 52:2995–3009. [PubMed: 9981373]
33. Guncar G, Wang CI, Forwood JK, Teh T, Catanzariti AM, Ellis JG, Dodds PN, Kobe B. The use of Co^{2+} for crystallization and structure determination, using a conventional monochromatic X-ray source, of flax rust avirulence protein. Acta Crystallogr Sect F Struct Biol Cryst Commun. 2007; 63:209–213.
34. Chivers PT, Tahirov TH. Structure of *Pyrococcus horikoshii* NikR: nickel sensing and implications for the regulation of DNA recognition. J Mol Biol. 2005; 348:597–607. [PubMed: 15826657]
35. Crane BR, Di Bilio AJ, Winkler JR, Gray HB. Electron tunneling in single crystals of *Pseudomonas aeruginosa* azurins. J Am Chem Soc. 2001; 123:11623–11631. [PubMed: 11716717]
36. Gasper R, Scrima A, Wittinghofer A. Structural insights into HypB, a GTP-binding protein that regulates metal binding. J Biol Chem. 2006; 281:27492–27502. [PubMed: 16807243]
37. Costello A, Periyannan G, Yang KW, Crowder MW, Tierney DL. Site-selective binding of Zn(II) to metallo-beta-lactamase L1 from *Stenotrophomonas maltophilia*. J Biol Inorg Chem. 2006; 11:351–358. [PubMed: 16489411]
38. Costello AL, Sharma NP, Yang KW, Crowder MW, Tierney DL. X-ray absorption spectroscopy of the zinc-binding sites in the class B2 metallo-beta-lactamase ImiS from Aeromonas veronii bv. sobria. Biochemistry. 2006; 45:13650–13658. [PubMed: 17087519]

NIH-PA Author Manuscript

NIH-PA Author Manuscript

NIH-PA Author Manuscript

39. Herbst RW, Guce A, Bryngelson PA, Higgins KA, Ryan KC, Cabelli DE, Garman SC, Maroney MJ. Role of conserved tyrosine residues in NiSOD catalysis: a case of convergent evolution. Biochemistry. 2009; 48:3354–3369. [PubMed: 19183068]
40. Giedroc DP, Arunkumar AI. Metal sensor proteins: nature's metalloregulated allosteric switches. Dalton Trans. 2007:3107–3120. [PubMed: 17637984]
41. Wirt MD, Sagi I, Chen E, Frisbie SM, Lee R, Chance MR. Geometric Conformations of Intermediates of B_{12} Catalysis by X-Ray Edge Spectroscopy - Co(I) B_{12}, Co(II) B_{12}, and Base-Off Adenosylcobalamin. J Am Chem Soc. 1991; 113:5299–5304.
42. Colpas GJ, Maroney MJ, Bagyinka C, Kumar M, Willis WS, Suib SL, Baidya N, Mascharak PK. X-Ray Spectroscopic Studies of Nickel-Complexes, with Application to the Structure of Nickel Sites in Hydrogenases. Inorg Chem. 1991; 30:920–928.
43. Kau LS, Spirasolomon DJ, Pennerhahn JE, Hodgson KO, Solomon EI. X-Ray Absorption-Edge Determination of the Oxidation-State and Coordination-Number of Copper -Application to the Type-3 Site in Rhus-Vernicifera Laccase and Its Reaction with Oxygen. J Am Chem Soc. 1987; 109:6433–6442.
44. Clark-Baldwin K, Tierney DL, Govindaswamy N, Gruff ES, Kim C, Berg J, Koch SA, Penner-Hahn JE. The limitations of X-ray absorption spectroscopy for determining the structure of zinc sites in proteins. When is a tetrathiolate not a tetrathiolate? J Am Chem Soc. 1998; 120:8401–8409.
45. Jacquamet L, Aberdam D, Adrait A, Hazemann JL, Latour JM, Michaud-Soret I. X-ray absorption spectroscopy of a new zinc site in the fur protein from *Escherichia coli*. Biochemistry. 1998; 37:2564–2571. [PubMed: 9485406]
46. Kuppuraj G, Dudev M, Lim C. Factors governing metal-ligand distances and coordination geometries of metal complexes. J Phys Chem B. 2009; 113:2952–2960. [PubMed: 19708219]
47. Jenkins RM, Singleton ML, Almaraz E, Reibenspies JH, Darensbourg MY. Imidazole-containing (N_3S)-Ni(II) complexes relating to nickel containing biomolecules. Inorg Chem. 2009; 48:7280–7293. [PubMed: 19572492]
48. Eicken C, Pennella MA, Chen X, Koshlap KM, VanZile ML, Sacchettini JC, Giedroc DP. A metal-ligand-mediated intersubunit allosteric switch in related SmtB/ArsR zinc sensor proteins. J Mol Biol. 2003; 333:683–695. [PubMed: 14568530]
49. Pennella MA, Arunkumar AI, Giedroc DP. Individual metal ligands play distinct functional roles in the zinc sensor *Staphylococcus aureus* CzrA. J Mol Biol. 2006; 356:1124–1136. [PubMed: 16406068]
50. Ma Z, Cowart DM, Ward BP, Arnold RJ, DiMarchi RD, Zhang L, George GN, Scott RA, Giedroc DP. Unnatural amino acid substitution as a probe of the allosteric coupling pathway in a Mycobacterial Cu(I) sensor. J Am Chem Soc. 2009; 131:18044–18045. [PubMed: 19928961]

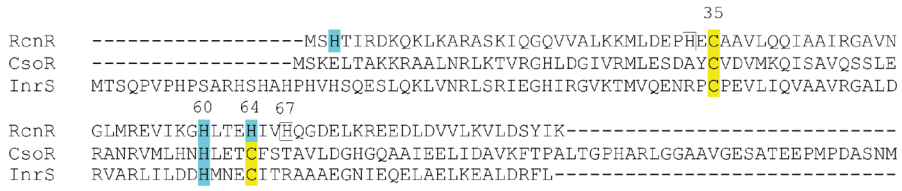

Figure 1.

Sequence alignment of *E. coli* RcnR, *M. tuberculosis* CsoR and *Synechocystis* PCC 6803 InrS generated using ClustalW (27). The metal binding residues of RcnR and CsoR are highlighted as well as the corresponding residues in InrS. Non conserved residues in RcnR are boxed.

NIH-PA Author Manuscript NIH-PA Author Manuscript NIH-PA Author Manuscript

NIH-PA Author Manuscript

NIH-PA Author Manuscript

NIH-PA Author Manuscript

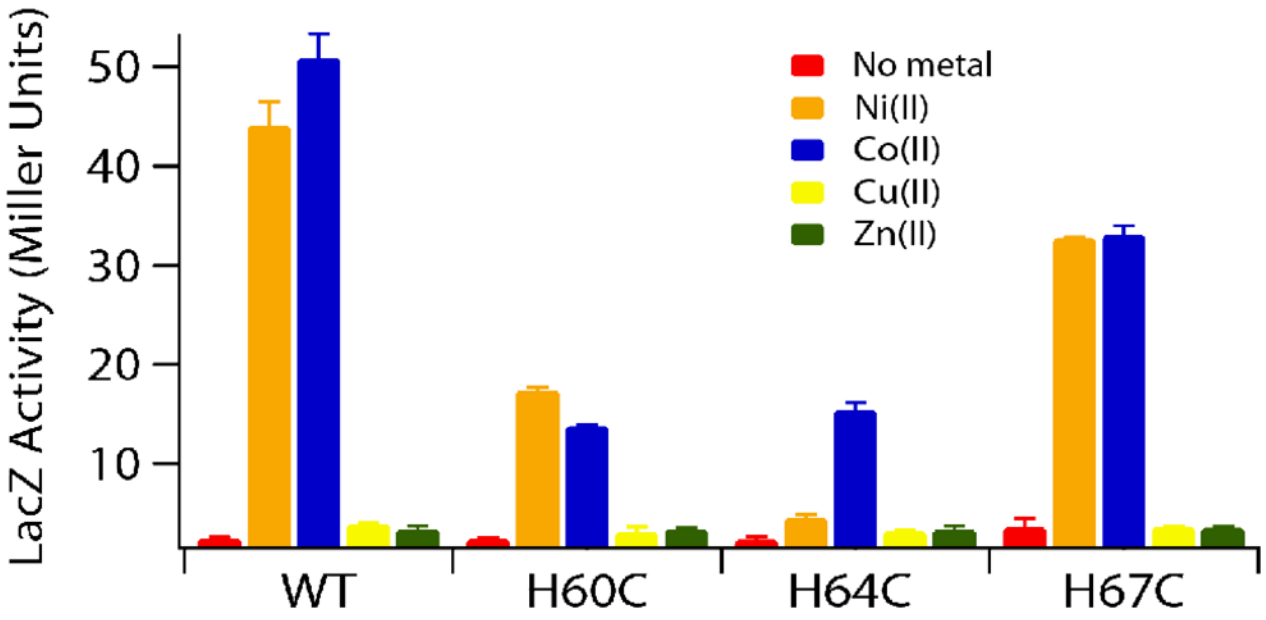

Figure 2.
LacZ reporter assay showing the effect of the H60C-, H64C- and H67C-RcnR mutations on the expression of P_{rcnA} in response to binding metal ions.

NIH-PA Author Manuscript
NIH-PA Author Manuscript
NIH-PA Author Manuscript

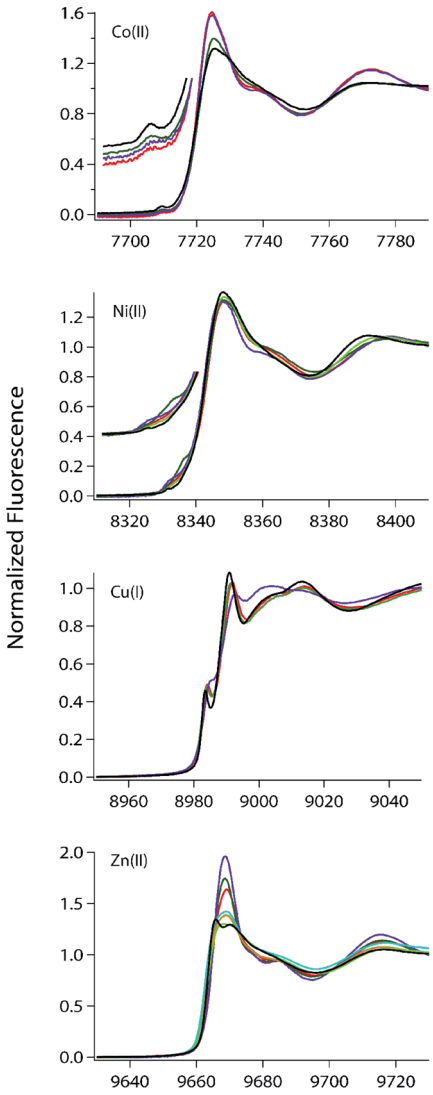

Figure 3.

XANES spectra of metal complexes of RcnR proteins in buffer with 20 mM Hepes, 300 mM NaBr and 10% glycerol: H60C (red), H64C (dark green), H67C (purple) and WT from ref. 25 (black). XANES spectra in buffer replacing NaBr with 300 mM NaOAc: H60C (orange), H64C (aqua), H67C (light green).

NIH-PA Author Manuscript
NIH-PA Author Manuscript
NIH-PA Author Manuscript

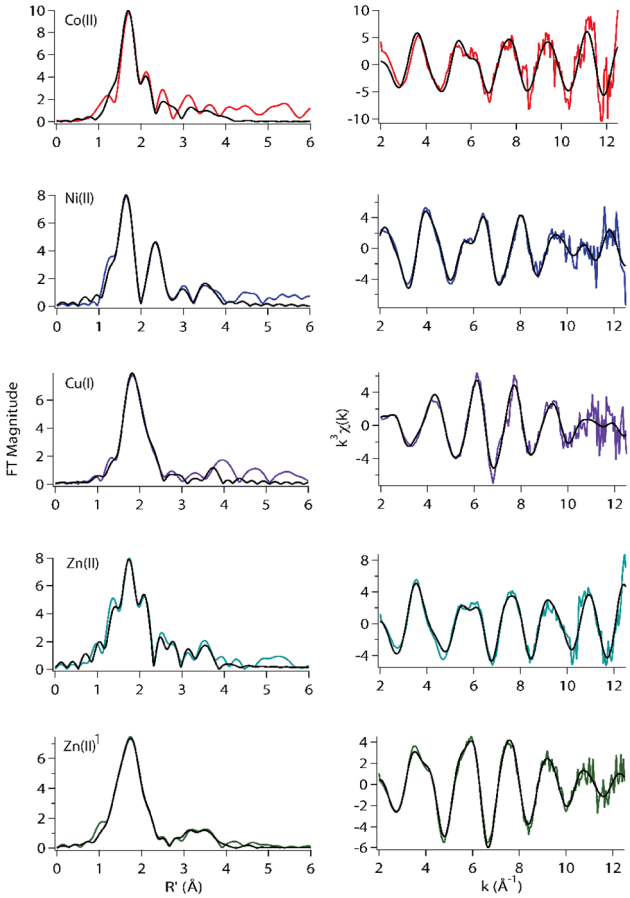

Figure 4.

K-edge XAS spectra of H60C RcnR metal complexes in buffer containing 20 mM Hepes, 300 mM NaBr/^{1}NaOAc and 10% glycerol at pH 7.0. For Cu(I), the buffer also contained 2 mM TCEP. Left: Fourier transformed EXAFS data (colored lines) and fits (black lines). Right: Unfiltered k^3-weighted EXAFS spectra and fits.

NIH-PA Author Manuscript

NIH-PA Author Manuscript

NIH-PA Author Manuscript

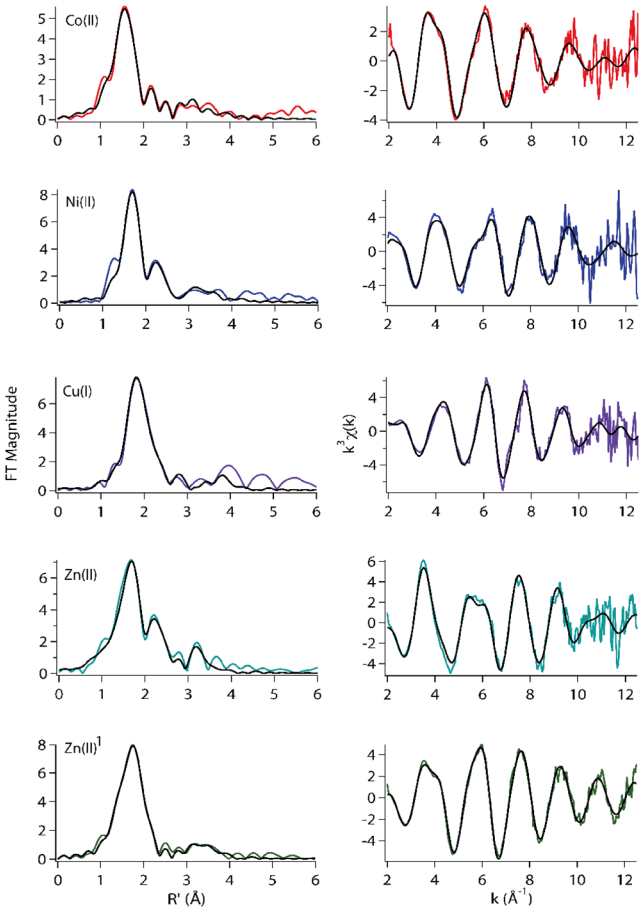

Figure 5.

K-edge XAS spectra of H64C-RcnR metal complexes in buffer containing 20 mM Hepes, 300 mM NaBr/[1]NaOAc and 10% glycerol at pH 7.0. For Cu(I), the buffer also contained 2 mM TCEP. Left: Fourier transformed EXAFS data (colored lines) and fits (black lines). Right: Unfiltered k^3-weighted EXAFS spectra and fits.

NIH-PA Author Manuscript
NIH-PA Author Manuscript
NIH-PA Author Manuscript

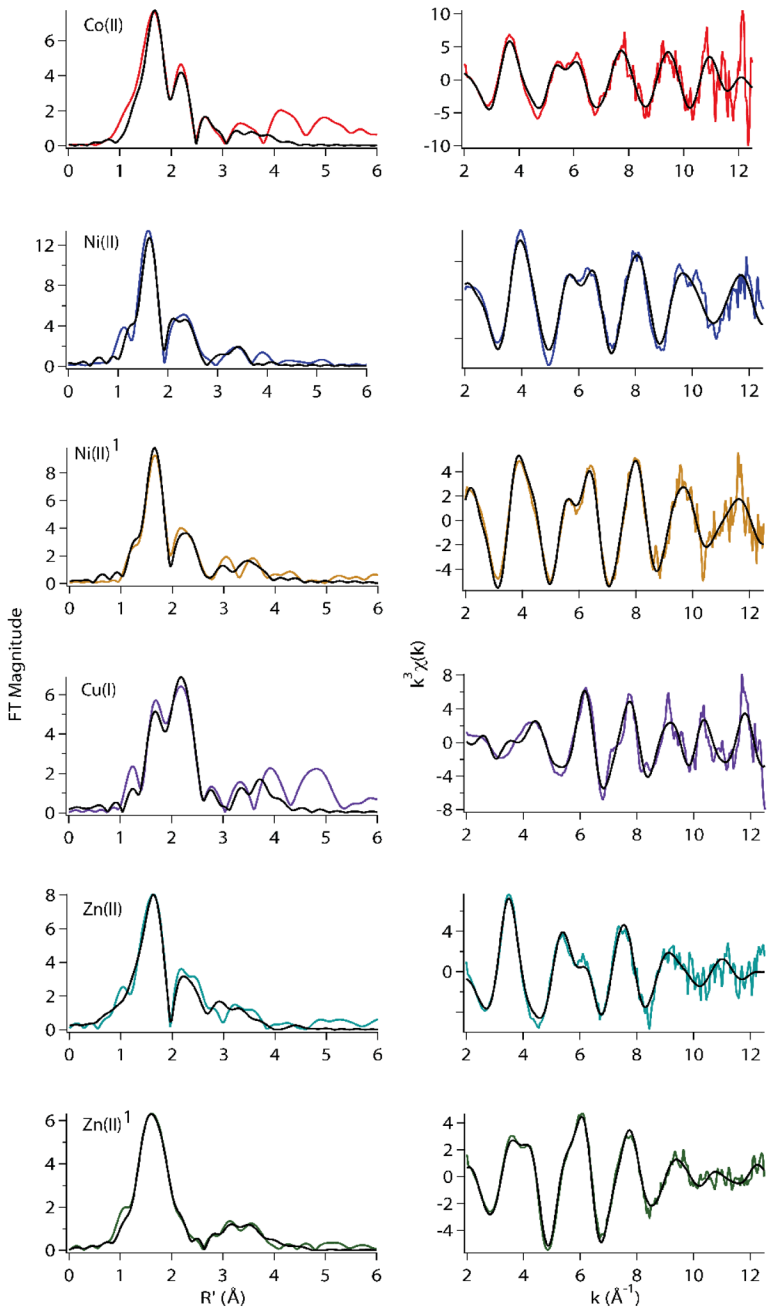

Figure 6.

K-edge XAS spectra of H67C RcnR metal complexes in buffer containing 20 mM Hepes, 300 mM NaBr/[1]NaOAc and 10% glycerol at pH 7.0. For Cu(I), the buffer also contained 2 mM TCEP. Left: Fourier-transformed EXAFS data (colored lines) and fits (black lines). Right: Unfiltered k^3-weighted EXAFS spectra and fits.

NIH-PA Author Manuscript NIH-PA Author Manuscript NIH-PA Author Manuscript

Table 1

XANES and EXAFS analysis for metal complexes of H60C-, H64C-, H67C-RcnR mutant proteins in buffer with 300mM NaBr.

	XANES Analysis				EXAFS Analysis					
Metal Ion	***K*-edge Energy (eV)**	**1s→3d Peak area (×10^2 eV)**	**1s→4pz Observed**	**CN#**	**Shell**	**r (Å)**	**σ^2 (×10^{-3} Å^2)**	**ΔE$_o$ (eV)**	**%R**	**Reduced χ^2**
				H60C-RcnR						
Co(II)	7720.6	13(3)	No	6	**5N/O (2Im)**	**2.13(1)**	**1.0(7)**	**0(2)**	**6.84**	**18.6**
					1S	**2.61(3)**	**4(3)**			
					5N/O (3Im)	2.13(1)	1.0(8)	0(2)	7.74	21.0
					1S	2.60(3)	4(4)			
Ni(II)	8343.7	5(1)	No	5/6	**5N/O (1Im)**	**2.080(7)**	**6.2(6)**	**11(1)**	**1.64**	**5.4**
					1S	**2.685(8)**	**1.0(7)**			
					5N/O (2Im)	2.079(7)	6.2(6)	10.4(9)	1.92	6.4
					1S	2.684(8)	0.9(7)			
Cu(I)	8987.3	NA	Yes	3	**2N/O (1Im)**	**2.13(2)**	**2(2)**	**5(2)**	**2.56**	**10.0**
					1S	**2.33(9)**	**7(6)**			
					1Br	**2.50(3)**	**7(2)**			
					2N/O (2Im)	2.13(2)	1(2)	6(2)	2.57	10.1
					1S	2.36(7)	8(7)			
					1Br	2.49(2)	7(3)			
Zn(II)	9665.1	NA	NA	6	**3N/O (2Im)**	**2.00(3)**	**8(2)**	**−9(3)**	**2.01**	**17.9**
					2S	**2.36(3)**	**1(3)**			
					1Br	**2.33(3)**	**0.2(13)**			
					3N/O (3Im)	2.00(4)	8(3)	−10(4)	2.10	18.7
					2S	2.35(3)	0.3(29)			
					1Br	2.32(3)	0.1(15)			
Zn(II)[1]	9662.6	NA	NA	5	**3N/O (1Im)**	**2.04(1)**	**6.8(7)**	**−8(1)**	**0.51**	**4.0**
					2S	**2.297(6)**	**4.5(3)**			
					3N/O (2Im)	2.04(1)	6.7(8)	−8(1)	0.53	4.1
					2S	2.299(7)	4.5(4)			
				H64C-RcnR						
Co(II)	7721.0	9(1)	No	6	**3N/O (3Im)**	**2.02(2)**	**6(1)**	**−8(3)**	**1.27**	**5.6**

NIH-PA Author Manuscript
NIH-PA Author Manuscript
NIH-PA Author Manuscript

	XANES Analysis				EXAFS Analysis					
Metal Ion	***K*-edge Energy (eV)**	**1s→3d Peak area (×10^2 eV)**	**1s→4pz Observed**	**CN#**	**Shell**	**r (Å)**	**σ^2 (×10^{-3} Å^2)**	**ΔE$_o$ (eV)**	**%R**	**Reduced χ^2**
					2S	**2.33(3)**	**9(1)**			
					1Br	**2.67(3)**	**6(2)**			
					3N/O (2Im)	2.03(2)	6(1)	−8(3)	1.38	6.0
					2S	2.33(3)	9(2)			
					1Br	2.67(3)	6(2)			
Ni(II)	8343.9	1.6(9)	Yes	4/5	**3N/O (3Im)**	**2.05(1)**	**3(1)**	**5(2)**	**2.63**	**7.7**
					1S	**2.31(3)**	**4(3)**			
					1Br	**2.69(5)**	**8(9)**			
					2N/O (2Im)	2.00(3)	3(3)	−3(4)	4.42	12.9
					1S	2.25(4)	0(2)			
					1Br	2.51(8)	6(6)			
Cu(I)	8987.1	NA	Yes	3	**2N/O (1Im)**	**2.12(2)**	**2(3)**	**4(2)**	**2.18**	**8.5**
					1S	**2.32(6)**	**6(5)**			
					1Br	**2.50(2)**	**7(2)**			
Zn(II)	9664.5	NA	NA	6	**3N/O (3Im)**	**2.05(2)**	**4(2)**	**−5(3)**	**1.81**	**11.0**
					2S	**2.40(4)**	**1(3)**			
					1Br	**2.36(4)**	**1(2)**			
					3N/O (2Im)	2.06(2)	4(1)	−5(2)	1.82	11.1
					2S	2.41(3)	3(3)			
					1Br	2.38(3)	2(2)			
Zn(II)[1]	9662.7	NA	NA	5	**3N/O (3Im)**	**2.02(1)**	**7.0(9)**	**−9(2)**	**0.67**	**10.6**
					2S	**2.280(7)**	**3.8(4)**			
					3N/O (2Im)	2.02(1)	7(1)	−9(2)	0.75	11.9
					2S	2.279(7)	3.8(4)			
				H67C-RcnR						
Co(II)	7720.8	13(2)	No	6	**3N/O**	**2.07(2)**	**2(1)**	**−4(2)**	**2.13**	**5.2**
					2N/O (3Im)	**2.20(2)**	**0(2)**			
					1S	**2.63(1)**	**1(1)**			
					3N/O	2.07(2)	2(2)	−3(2)	2.18	5.3
					2N/O (2Im)	2.20(2)	0(2)			

NIH-PA Author Manuscript
NIH-PA Author Manuscript
NIH-PA Author Manuscript

	XANES Analysis				EXAFS Analysis					
Metal Ion	***K*-edge Energy (eV)**	**1s→3d Peak area (×10^2 eV)**	**1s→4pz Observed**	**CN#**	**Shell**	**r (Å)**	**σ^2 (×10^{-3} Å^2)**	**ΔE$_o$ (eV)**	**%R**	**Reduced χ^2**
					1S	2.63(1)	1(1)			
Ni(II)	8343.3	5(1)	No	5/6	5N/O (3Im)	2.05(1)	2.1(9)	5(2)	6.81	98.0
					1S	2.7(1)	5(11)			
					5N/O (2Im)	**2.06(1)**	**2(1)**	**6(2)**	**7.15**	**102.9**
					1S	**2.62(8)**	**6(8)**			
Ni(II)[1]	8343.1	3(1)	No	6	**5N/O (2Im)**	**2.083(6)**	**3.8(5)**	**9(1)**	**2.23**	**16.3**
					1S	**2.67(2)**	**4(2)**			
					5N/O (3Im)	2.083(7)	3.8(5)	9(1)	2.55	16.5
					1S	2.67(2)	4(2)			
					5N/O (1Im)	2.083(7)	3.8(5)	9(1)	2.27	16.6
					1S	2.67(2)	3(2)			
Cu(I)	8984.9	NA	Yes	3	**1N/O (1Im)**	**2.04(3)**	**0(3)**	**5(5)**	**5.45**	**45.4**
					1S	**2.31(5)**	**3(3)**			
					1Br	**2.51(2)**	**3(2)**			
Zn(II)	9665.0	NA	NA	6	**4N/O**	**2.15(2)**	**6(1)**	**5(2)**	**2.63**	**26.2**
					1N/O (2Im)	**1.90(4)**	**14(4)**			
					1S	**2.69(4)**	**8(5)**			
					4N/O	2.14(2)	5(1)	4(2)	2.64	26.3
					1N/O (3Im)	1.90(4)	14(5)			
					1S	2.69(6)	11(8)			
Zn(II)[1]	9663.6	NA	NA	4	**2N/O (1Im)**	**1.981(8)**	**3.6(6)**	**−9(1)**	**0.61**	**13.6**
					2S	**2.271(7)**	**6.0(4)**			
					2N/O (2Im)	1.980(9)	3.6(6)	−9(1)	0.61	13.7
					2S	2.271(8)	6.0(4)			

[*] EXAFS fits in **bold** type are shown in Figures 4–9.

[1] Sample prepared in buffer with 20 mM Hepes, 300 mM NaOAc and 10 % Glycerol at pH 7.0.

The numbers in parentheses are the estimated uncertainties in the corresponding variable. These uncertainties are calculated by SixPack and reflect the change in variable that will result in an increase in χ^2 of 1.